Macromolecules

Article

pubs.acs.org/Macromolecules

Architecture-Induced Size Asymmetry and Effective Interactions of Ring Polymers: Simulation and Theory

Arturo Narros,*[,†] Angel J. Moreno,[‡,§] and Christos N. Likos[†]

[†]Faculty of Physics, University of Vienna, Boltzmanngasse 5, A-1090 Vienna, Austria

[‡]Centro de Física de Materiales (CSIC, UPV/EHU) and Materials Physics Center MPC, Paseo Manuel de Lardizabal 5, E-20018 San Sebastián, Spain

[§]Donostia International Physics Center, Paseo Manuel de Lardizabal 4, E-20018 San Sebastián, Spain

ABSTRACT: We investigate, by means of Monte Carlo simulations, the role of ring architecture and topology on the relative sizes of two interacting polymers as a function of the distance between their centers-of-mass. As a general rule, polymers swell as they approach each other, irrespectively of their topologies. For each mutual separation, two identical linear polymers adopt the same average size. However, unknotted rings at close separations adopt different sizes, with the small one being "nested" within the large one over long time intervals, exchanging their roles in the course of the simulation. For two rings of different architectures and identical polymerization degree, the knotted one is always smaller, penetrating the unknotted one. On the basis of these observations, we propose a phenomenological theory for the effective interactions between rings, modeling them as unequal-sized penetrable spheres. This simple approximation provides a good description of the simulation results. In particular, it rationalizes the non-Gaussian shape and the short-distance plateau observed in the effective potential between unknotted ring polymers and pairs of unequal-sized unknotted/knotted ones. Our results demonstrate the crucial role of the architecture on both the effective interactions and the molecular size for strongly interpenetrating polymers.

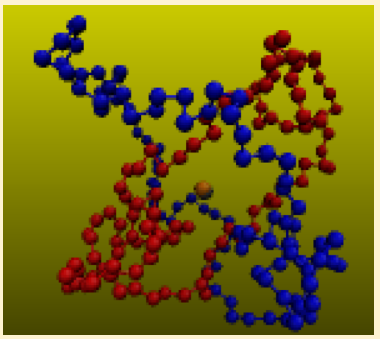

1. INTRODUCTION

Molecular architecture and topology have a deep impact in the physical properties of polymer solutions and melts. An archetypical example is that of ring polymers. The simple operation of joining permanently the two ends of a linear chain strongly affects its thermodynamic and dynamic properties. To cite a few, some striking differences between rings and their linear counterparts with *identical* chemical composition and degree of polymerization are (a) rings polymers in solution exhibit a different θ-point than their linear counterparts,[1,2] (b) the stress relaxation modulus of melts of entangled rings does not exhibit the usual plateau regime characteristic of their linear counterparts, but a broad power-law decay,[3] and (c) the effective potential $V_{\mathrm{eff}}(R)$ between rings in solution is non-Gaussian,[4,5] in contrast to the effective Gaussian interaction between linear chains.[5−16]

Coarse-graining is a powerful methodology to investigate the physical properties of polymer solutions. By removing most of the internal degrees of freedom and retaining a few ones (usually the three coordinates of the center-of-mass), the macromolecular solution is reduced to an effective fluid of ultrasoft particles. The investigation of the effective fluid provides an efficient and economical route toward the structural and thermodynamic properties of the real solution.[17,18] Since macromolecular centers-of-mass are allowed to coincide without violating excluded-volume interactions between monomers, the effective ultrasoft potential is bounded; i.e., it does not diverge at any separation between the centers-of-mass. The first investigation on effective potentials for polymers in solution was focused in linear chains. Computer simulations confirmed the Gaussian functional form of the potential[5−16] put forward by early theoretical approaches[8,19] and by renormalization-group arguments.[9]

During the past years, a series of computational works have investigated the effective potentials $V_{\mathrm{eff}}(R)$ between ring polymers in good solvent conditions, where R stands for the distance between their centers-of-mass. As mentioned above, the effective potential carries the signature of the ring architecture and exhibits a non-Gaussian profile,[4,5] unlike the Gaussian potential found for their chemically identical linear counterparts. The qualitative features of the effective potential in good solvent are independent of the specific microscopic interactions between monomers. Very recently, the same features have also been observed for semiflexible rings, confirming the universality of the intrinsically non-Gaussian character of the interaction.[20] This includes a "plateau" at short separation between centers-of-mass and, for small molecular weights, a minimum at zero separation. A consequence of the latter is the formation of cluster crystals in the effective fluid at high densities.[21,22] However, these phases are predicted for densities far beyond the overlap concentration, where intervening many-body effects alter the effective interaction

Received: August 6, 2013
Revised: November 12, 2013
Published: November 22, 2013

dx.doi.org/10.1021/ma4016483 | *Macromolecules* 2013, 46, 9437−9445

derived in the limit of high dilution. Indeed, flexible ring polymers progressively shrink in the concentrated regime, a feature that prevents the formation of clusters in the real solution,[5] and the shrinking of their size with concentration above the overlap density has been found to follow a stronger power law than that of their linear counterparts.[23,24] In the case of semiflexible rings, shrinking involves a strong energetic penalty. Thus, they are weakly deformed and even swell by increasing concentration, which favors interpenetration and clustering. However, the clusters in the real solution have a strongly elongated, anisotropic character, different from the isotropic structure predicted by the effective potential.[20] This suggests that the mutual orientation between semiflexible rings plays a crucial role in the effective interaction, and a formulation only in terms of the centers-of-mass is incomplete. Having noted this, the effective potentials for both flexible and semiflexible rings still provide an accurate description of the correlations between centers-of-mass from high dilution up to the overlap concentration ρ^*. Even a semiquantitative description is achieved at densities somewhat higher than ρ^*.[5,20]

Several theoretical works have separated the effective interaction between ring polymers into a topological and a self-avoidance contribution. This was first proposed by Frank-Kamenetskii et al.[25] Later, Tanaka[26] and Iwata[27] reproduced the plateau feature of $V_{\text{eff}}(R)$ by analytical calculations, combining Gaussian statistics of the intramolecular conformations with the Gaussian linking number. Bohn and Heermann[4] and Hirayama,[28] by using on-lattice and off-lattice simulations, respectively, demonstrated the relatively low influence that the topological contribution has on $V_{\text{eff}}(R)$ at overlapping configurations. In particular, Hirayama[28] showed that actually the topological contribution was strongly coupled to the self-avoidance parameter.

Little attention has been paid to a feature that may play a crucial role in the qualitative differences between the effective potentials of rings and linear chains. This is the effect of architecture on the polymer conformations at overlapping configurations. Indeed, the typical conformations should determine the number of contacts between monomers, and consequently the value of the effective potential, at each separation between centers-of-mass. In this article we investigate this feature in detail. We find that polymers swell as they approach each other. However, whereas two identical linear polymers adopt roughly the same average size, identical unknotted rings at close separations adopt different sizes, with the small one being "nested" within the large one over long time intervals, exchanging their roles in the course of the simulation. For two rings of different topologies and identical polymerization degree, the knotted one is always smaller, penetrating the unknotted one. On the basis of these results, we propose a simple yet accurate theory for the effective interaction between rings, modeling them as unequal penetrable spheres. This picture provides a good description of the simulation results, and it rationalizes the non-Gaussian shape and the short-distance plateau observed in the effective potential for ring polymers.

The article is organized as follows: In section 2 we give simulation details and define size parameters characterizing polymer conformations. In section 3 we present results for effective potentials and size parameters, for various lengths and topologies of the two polymers. In section 4 we introduce the theoretical approach for the effective interaction and compare theoretical predictions with the simulation results. Conclusions are given in section 5.

2. SIMULATION MODEL AND SIZE PARAMETERS

We have computed the effective potential $V_{\text{eff}}(R)$ for the interaction between two polymers A and B as a function of the distance between their centers-of-mass, R. The choice of the latter as effective coordinates to describe the whole polymer is despite its appeal due to symmetry, an arbitrary one. Indeed, linear polymers can be coarse-grained in a number of ways, and although the center-of-mass choice is the most common one,[6−12,14−16] the end monomer or the central monomers have also been employed as effective coordinates in the past.[13] Similarly, in a recent work the monomers of closest approach between two rings have been used to coarse-grain the polymers,[29] a choice that results in a logarithmically diverging, entropic repulsion between the rings—a feature common also to linear and star polymers.[17]

Each of the two polymers in this work has linear or ring topologies, and in the latter case they can be knotted or unknotted. By denoting their topology and polymerization degree as τ_i and N_i, respectively, with $i \in \{\text{A, B}\}$, the effective potential is a function of all the former parameters, i.e., $V_{\text{eff}} = V_{\text{eff}}(R,\tau_A,N_A,\tau_B,N_B)$. The topological index assumes, in this work, values $\tau \in \{L, 0_1, 3_1\}$, where L stands for the linear chain topology, 0_1 for the unknotted rings (trivial knots), and 3_1 for the trefoil knot.

We employed for all polymers examined in this work a hard-sphere-tether model to describe intermonomer interactions and connectivity. Monomers are modeled as hard spheres of diameter σ and the connections among them are implemented as threads of maximal surface-to-surface extension $\delta\sigma$ ($\delta > 1$), as in ref 5. Accordingly, the monomer−monomer interaction $V_{\text{mm}}(r)$ and the bonding interaction $V_{\text{bond}}(r)$, where r is the distance between the monomer centers, read as

$$V_{\text{mm}}(r) = \begin{cases} \infty & \text{for } \dfrac{r}{\sigma} < 1 \\ 0 & \text{for } \dfrac{r}{\sigma} > 1 \end{cases} \tag{1}$$

acting among all monomers and

$$V_{\text{bond}}(r) = \begin{cases} \infty & \text{for } \dfrac{r}{\sigma} < 1 \\ 0 & \text{for } 1 < \dfrac{r}{\sigma} < 1 + \delta \\ \infty & \text{for } \dfrac{r}{\sigma} > 1 + \delta \end{cases} \tag{2}$$

for connected ones. We prevent crossing of the bonds of the rings, and thus conservation of all the intra- and intermolecular topological constraints (no modification of the knotedness and no accidental catenations), by setting $\delta = 0.2$ and choosing the Monte Carlo displacement step to be less than or equal to δ. We have explicitly checked the avoidance of spurious catenations by creating a pair of catenated rings, pulling each of them with opposite forces and verifying that they never disentangle, no matter how strong the applied force is.

The moves employed in our Monte Carlo simulations were mostly simple attempts to move single monomers of the polymers. We define as a Monte Carlo cycle a set of N single-monomer attempted moves, where N denotes the degree of

dx.doi.org/10.1021/ma4016483 | Macromolecules 2013, 46, 9437−9445

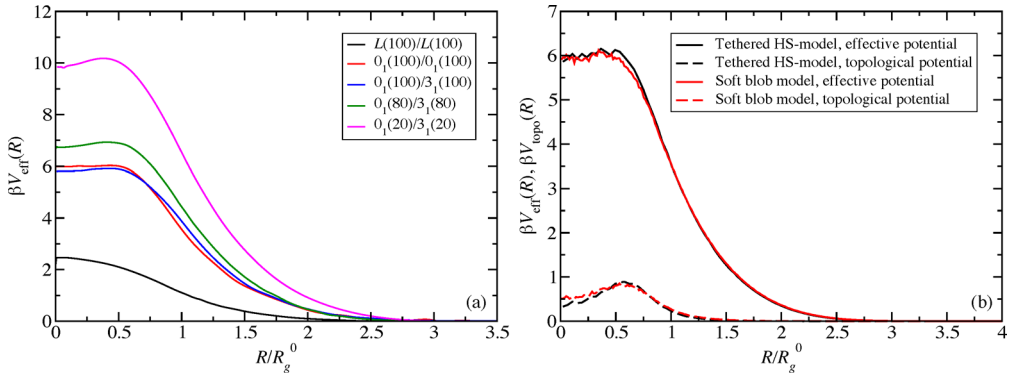

Figure 1. (a) Center-of-mass effective $V_{\text{eff}}(R)$ for different combinations of topologies and sizes (see legend). Here, $\beta = (k_B T)^{-1}$, with k_B the Boltzmann constant and T the absolute temperature. (b) Effective potential between the centers-of-mass of two $0_1/0_1$ rings resulting from two microscopically different models (see text) as well as the topological potential between the same resulting from these models.

polymerization of the molecule. To make sure that configurations on which measurements have been taken are fully decorrelated from one another, we make, for the rings, one measurement in every $N_{\text{meas}} = 5000$ MC cycles and we denote N_{meas} as one MC measurement cycle. Typical simulation runs for the rings were $N_{\text{run}} = 5 \times 10^7$ MC cycles long, both for isolated polymers and for interacting ones. For linear chains, the extension of the measurement cycles was shorter, $N_{\text{meas}} = 1000$ MC cycles, since in this case bond crossing is allowed, and thus we can apply bigger monomer displacements, resulting into faster decorrelation of the configurations. The quantities measured were the gyration radii for different interpolymer separations as well as the effective interaction potential $V_{\text{eff}}(R)$ as a function of the separation R between the polymers' centers-of-mass.

The effective potentials were determined from Monte Carlo simulations by using the umbrella-sampling technique, as explained in ref 5, to measure the probability $P(R)$ of finding the centers-of-mass of the rings at separation R, deriving then the effective pair potential as

$$\beta V_{\text{eff}}(R) = -\ln\left[\frac{P(R)}{P(R \to \infty)}\right] \tag{3}$$

To ensure proper sampling throughout the range of separations $R/R_g^0 \in [0, 12]$, the whole R interval was split into 20−30 windows of width $w \cong 0.3R_g^0$ each, where R_g^0 is defined in eq 6. Results from successive windows were matched as described in ref 5. Occasionally, small rigid rotations of the whole molecule for large distances R were also employed in MC; however, pivoting moves, such as *crankshaft*, were not implemented for the rings, given the small size of the molecules and, therefore, the low probability of acceptance for small values of R.

As will be shown in the following, the specific architectures of the two polymers have also a deep impact on their size at close separation. Consider, for instance, the radius of gyration $R_{g,i}$ of the polymer i, while the center-of-mass of the other polymer, $j \neq i$ and $i, j \in \{A, B\}$, is kept at a distance R from the center-of-mass of polymer i. Denoting with $\mathbf{r}_{k,i}$, $k = 1, 2, \ldots, N_i$, the instantaneous positions of the monomers of polymer i, we have

$$R_{g,i}^2 = \left\langle \frac{1}{N_i^2} \sum_{k=1}^{N_i} \sum_{l=k+1}^{N_i} (\mathbf{r}_{k,i} - \mathbf{r}_{l,i})^2 \right\rangle_{R,j} \equiv \langle \hat{R}_{g,i}^2 \rangle_{R,j} \tag{4}$$

where the angular brackets $\langle \cdots \rangle$ denote a statistical average over all polymer conformations and the subscript (R, j) is a reminder of the existence of a fluctuating polymer j at distance R from the polymer i. Equation 4 serves also as the definition of the instantaneous radius of gyration $\hat{R}_{g,i}$ of the polymer.

It becomes evident that $R_{g,i}$ depends not only on the architecture and size of the polymer i itself but also on the same characteristics of polymer j *and* on the separation between the two: $R_{g,i} = R_{g,i}(R; \tau_A, N_A, \tau_B, N_B)$. We further define the unperturbed radius of gyration $R_{g,i}^0(\tau_i, N_i)$ of the polymer i as its value at infinite separation from polymer j:

$$R_{g,i}^0(\tau_i, N_i) \equiv R_{g,i}(R \to \infty; \tau_A, N_A, \tau_B, N_B) \tag{5}$$

In the following, results will be presented by normalizing the separation R by the arithmetic mean, R_g^0, of the unperturbed radii of gyration of the two polymers:

$$R_g^0 \equiv \frac{R_{g,A}^0(\tau_A, N_A) + R_{g,B}^0(\tau_B, N_B)}{2} \tag{6}$$

Finally, we order the polymers at every separation into a smaller and a larger one, according to the value of their gyration radius, and we use the greek index $\gamma \in \{<,>\}$ to denote the two, respectively. A useful quantity that will be discussed is the swelling ratio of the polymer γ, defined as

$$\alpha_\gamma(R; \tau_A, N_A, \tau_B, N_B) \equiv \frac{R_{g,\gamma}(R; \tau_A, N_A, \tau_B, N_B)}{R_{g,\gamma}^0(\tau_\gamma, N_\gamma)} \tag{7}$$

i.e., as the ratio between the perturbed and the unperturbed size of the polymer. As will be demonstrated, this quantity has also a strong dependence on the specific topologies of the two polymers. Having established the dependence of the former quantities on $\tau_{A,B}$ and $N_{A,B}$, in the following we simplify the notation, leaving the distance R between centers-of-mass as the only explicit parameter.

3. RESULTS

Results for the effective potentials from our simulations are shown in Figure 1a. These are given for several topologies and polymerization degrees of the two polymers. When both them are linear chains, $V_{\text{eff}}(R)$ has a Gaussian shape (black line). This result is related to the Gaussian character of the distribution of monomers around their centers-of-mass.[30] Renormalization-group studies have shown that the shape is indeed of Gaussian form,[9] whereas its amplitude (i.e., the value it attains at zero

dx.doi.org/10.1021/ma4016483 | Macromolecules 2013, 46, 9437−9445

separation) has been shown to be independent of the degree of polymerization,[8] in contrast to earlier, mean-field predictions of Flory and Krigbaum,[19] who were, nevertheless, the first to propose such an interaction as early as in 1950. This potential of mean force has been confirmed by a number of on- and off-lattice simulations ever since.[5−16] Its shape is universal, i.e., independent of the underlying microscopic model, when R is scaled with the gyration radius, provided that the degree of polymerization exceeds a threshold value N_L^* that depends on the model; for off-lattice models, typically $N_L^* \sim 100$. Its amplitude in this scaling limit is $V_{eff}(R=0) \cong 2k_BT$. Scaling behavior of $V_{eff}(R)$ has also been found for rings at $N > N_{0_1}^* \sim 100$, though in this case the observed amplitude of the potential is different, $V_{eff}(R=0) \cong 6k_BT$.[5] Hence, for a same polymerization degree, the effective potential between ring polymers is much more repulsive than for their linear counterparts. Another remarkable difference with the case of linear chains is that $V_{eff}(R)$ for unknotted polymers does not have a Gaussian shape.[4,5,28] Instead, it features a plateau at small separations, and even a minimum at $R = 0$ for small polymerization degrees $N < N_{0_1}^*$. This feature is intimately connected to the typical configurations of interpenetrated rings, in which one ring adopts an open conformation allowing the other to stay in the center of the former for long intervals (see below).

The plots in Figure 1a further demonstrate that the non-Gaussian character observed for the effective potential between rings is not limited to the simplest case of two unknotted circular polymers but is also found for combinations of different topologies. This is illustrated there for pairs of rings with the same N, but distinct topologies 0_1 and 3_1. As observed for the case of two unknotted rings, the potential can exhibit a minimum at $R = 0$. Interestingly, for sufficiently large rings ($N = 100$) we find essentially the same interaction for distinct rings, $\tau_A = 0_1$ and $\tau_B = 3_1$, as for identical unknotted rings $\tau_A = \tau_B = 0_1$ (compare red and blue lines). Although $N = 100$ is already sufficiently large for the effective interaction between 0_1 rings to be in the scaling regime, the close resemblance with the $0_1/3_1$ interaction is at this point a matter of coincidence: for a knotted ring, the degree of polymerization is too small for the knot to be irrelevant. At the limit $N \to \infty$, knots become weakly localized in three spatial dimensions:[31] there, we can surmise that the effects of (simple) knots on the rings will renormalize away, since their typical size R_k scales as $R_k \sim N^{0.75}$ and therefore $R_k/R_g \to 0$ as $N \to \infty$.

The insensitivity of the $0_1/0_1$ effective potential $V_{eff}(R)$ to the underlying microscopic model for a degree of polymerization $N = 100$ is demonstrated in Figure 1b. In addition to the HS-tethered model described above, we have also considered 0_1-ring polymers consisting of $N = 100$ soft blobs and renormalized elastic spring interactions, which result from a coarse-graining of a large number of underlying monomers.[32] We have repeated the calculation with the soft model, for which catenations are not excluded a priori, and thus every configuration has to be checked for its topological legitimacy. Following ref 4, we apply the Gaussian linking number W as a diagnostic tool for catenations, and all configurations of catenated rings are thus rejected. Similarly, the topological potential $V_{topo}(R)$ shown in Figure 1b is also insensitive to the microscopic model details, confirming that $N = 100$ is a sufficiently large degree of polymerization for 0_1 rings, leading to universal results for the effective interactions.

Insight into the microscopic mechanism leading to the features observed in the effective potential can be gained by monitoring the evolution of the size of both rings at full overlap. Figure 2 shows results, plotted against the number of

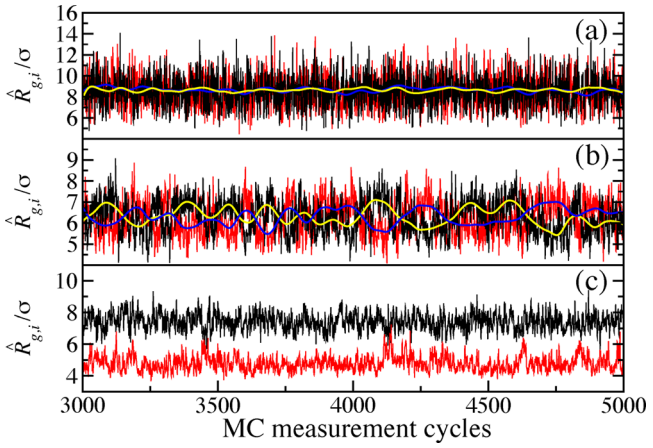

Figure 2. Instantaneous value of the radius of gyration $\hat{R}_{g,i}$, i = A, B, for two selected polymers A and B at full interpenetration ($R = 0$), against the number of MC measurement cycles for already equilibrated configurations. In all cases the degree of polymerization is $N_A = N_B = 100$ for both polymers. The topologies of the two polymers are (L, L), (0_1, 0_1), and (0_1, 3_1) for (a), (b), and (c), respectively. The instantaneous values $\hat{R}_{g,i}$ for each polymer are represented in black and red colors. In the case of the topologically different rings in (c), black and red lines correspond to the 0_1 and 3_1 ring, respectively. The smooth yellow and blue lines in (a) and (b) are averages, over intervals of 100 consecutive points, of the black and red lines, respectively.

MC measurement cycles, for the instantaneous radii of gyration of the two polymers at mutual distance $R = 0$. All results correspond to identical degree of polymerization, $N = 100$, for both rings. The three panels present results for different combinations of topologies: $\tau_A = \tau_B = L$ in Figure 2a; $\tau_A = \tau_B = 0_1$ in Figure 2b; and $\tau_A = 0_1$, $\tau_B = 3_1$ in Figure 2c. As can be seen in the latter case, the knotted rings are systematically smaller than their unknotted counterparts. This is not surprising, since this is indeed also the case when both polymers are isolated ($R \to \infty$). As expected, polymers with same N and τ (Figure 2a,b) may adopt different instantaneous sizes, but for long enough times they show the same average size. However, size fluctuations behave rather differently for linear and ring polymers. In the case of two identical fully interpenetrated rings, one is systematically smaller than the other over relatively long time intervals (Figure 2b). This effect can be better visualized by smoothing the curves of the instantaneous values of $\hat{R}_{g,i}$'s (black and red) over intervals of 100 MC measurement cycles, leading to the yellow and blue curves in Figure 2a,b. This feature reflects the fact that for relatively long time intervals one of the unknotted rings adopts an open configuration, leaving free space for penetration by the other ring. The exchange of the roles of the two rings takes place at intervals of the order of the Rouse time for rings of $N = 100$.

In Figure 3, we show the swelling ratio $\alpha_\gamma(R)$ as a function of the distance between centers-of-mass R, for several combinations of architectures (linear/ring) and topologies (knotedness of rings). In all cases represented in the figure, the two polymers have *identical* N. Dashed lines with empty symbols correspond to the "small" polymer, whereas solid lines with filled symbols correspond to the "large" one. In the case of

dx.doi.org/10.1021/ma4016483 | *Macromolecules* 2013, 46, 9437−9445

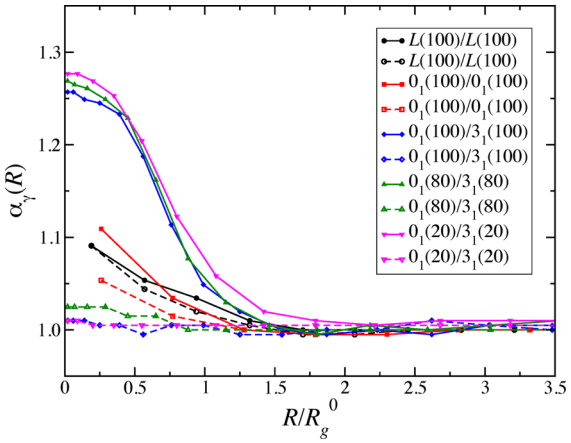

Figure 3. Swelling ratios of the two polymers as a function of the normalized distance between their centers-of-mass. Data are shown for different combinations of the topologies and polymerization degrees (see legend). Full symbols joined by solid lines are data for the large polymer. Empty symbols joined by dashed lines are data for the small polymer. See text for the definitions of "large" and "small" polymer.

distinct topologies (0_1 and 3_1 rings, see caption), the "large" and "small" polymers are the unknotted and knotted ring, respectively. Indeed, for identical N, 3_1 rings are on average smaller than 0_1 rings. In the case of identical architectures, "small" and "large" refer to the *instantaneously* smaller and larger polymer, respectively, and the averages in eq 7 are calculated according to this criterion instead of averaging over the same polymer. Indeed, as illustrated in panels a and b of Figure 2, the identities of the large and small polymer alternate during the simulation because of intramolecular fluctuations.

As expected, the swelling parameter is equal to unity at long separations, $R \gg R_g^0$, when there is no overlap between the two polymers. However, by increasing interpenetration (decreasing R), the swelling ratios of the large and small polymer become rather different. In the case of the mixed topologies, the size of the small polymer (3_1 knot) is essentially unperturbed by interpenetration with the large polymer (unknotted 0_1 ring). However, the large polymer strongly swells, up to about a 25% at full overlap ($R = 0$). This effect seems to be weakly dependent on the degree of polymerization—note the close agreement between the data sets for $20 \leq N < 100$. These results show that in entropic terms it is more favorable to swell the unknotted ring, leaving free space to accommodate the unperturbed knotted ring, than to swell the knotted ring, which would involve localization of the knot. In the case of the $0_1/0_1$ pair, *both* polymers show a significant swelling at strong interpenetration. However, the swelling ratio is smaller than for the unknotted rings in the $0_1/3_1$ pairs. In the case of identical linear chains, the "large" and "small" polymers are affected almost identically by interpenetration and show very similar swelling factors, whereas in the case of 0_1 rings, it is clear that there is a significant size discrepancy between the two, in line with the results presented in Figure 2b. Here, it is worth pointing out that Bohn and Heermann[4] also calculated a swelling ratio for two interacting rings, albeit without splitting them into a smaller and a larger one but rather by averaging over the two sizes. Our results are in full agreement with those in ref 4: a gradual swelling of the rings for distances $R/R_g^0 \lesssim 1.5$, reaching a maximum value of $\langle\alpha\rangle \cong 1.12$ at $R = 0$, has been found there, which compares very well with our own results in Figure 3. Furthermore, the analysis of relative orientation between the 0_1 rings in ref 4 confirms our assertion that two interpenetrating rings assume a threading conformation with nearly perpendicular mutual orientation.

We have also calculated the local density of monomers, $\rho(r)$, where r is the distance to the center-of-mass of the polymer. Figure 4 shows results for $\rho(r)$ when two identical polymers of $N = 100$ monomers are fully interpenetrated ($R = 0$, solid lines) or isolated ($R \to \infty$, dashed lines). Panels a and b show results for linear chains and unknotted rings, respectively. As in the case of the swelling ratio for identical polymers (see above), we present results by performing averages over the *instantaneously* "large" (black lines) and "small" polymer (red lines). Full interpenetration affects the monomer densities of linear chains and rings in a very different way. A moderate distortion of the unperturbed density profile ($R \to \infty$) is found for the linear chains, increasing the intensity at long r. A similar effect is found for the small ring in the case of fully interpenetrated rings. However, a strong distortion is found for the large ring. The monomer density of the large ring at full overlap does not show the monotonous decay observed for all the isolated polymers ($R \to \infty$) and for the rest of the cases at $R = 0$ that are shown in Figure 4. Instead, it shows a maximum at a finite distance from the center-of-mass. This feature is consistent with

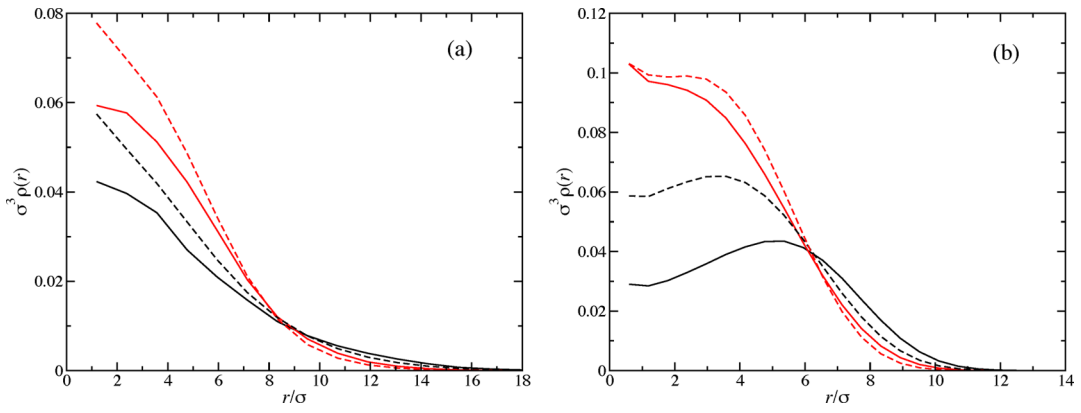

Figure 4. Monomer distributions (density profiles) of the two polymers. Solid and dashed lines are data for full interpenetration ($R = 0$) and for infinite separation ($R \to \infty$), respectively, with R the distance between the centers-of-mass of the polymers. Black and red color codes correspond to the large and small polymer, respectively. In all cases the polymerization degree is $N = 100$. Panel a shows data for two linear chains, (L, L). Panel b shows data for two unknotted rings, (0_1, 0_1).

dx.doi.org/10.1021/ma4016483 | *Macromolecules* 2013, 46, 9437−9445

the observations for the swelling ratio (see Figure 3) and reflects the open conformations adopted by the large ring, leaving free space for accommodating the small ring. Although we do not deal in this work with knots of higher complexity, it is worth mentioning that for an interacting $5_1/5_1$ pair of N = 100 monomers each, the density profiles at $R \to \infty$ and those at $R = 0$ are very different, an effect of the fact that this degree of polymerization is too low. Consequently, about one-third of the monomers are within the knot, and they cause large deviations from the universal behavior expected for $N \to \infty$. The same holds to a lesser degree for $3_1/3_1$ pairs with $N = 100$ monomers each as well. The theoretical model in section 4 does not, therefore, apply to these cases.

All the results presented in this section reveal an interesting phenomenon for all polymer architectures: the swelling of at least one of the two polymers at full interpenetration, adapting its size and shape to accommodate the other polymer. This feature, which may lead to a minimum at $R = 0$ for $V_{\text{eff}}(R)$, can be seen as a "soft depletion effect" of the monomers from the centers of mass of the ring to which they belong. In the case of the ring polymers, the depletion is induced by the monomers of the small polymer on those of the large one. Instead, soft depletion is a mutual effect for linear chains (both chains swell, see Figure 3).

4. THEORETICAL MODEL OF THE RING POLYMER EFFECTIVE POTENTIAL

Following the ideas of Grosberg et al.,[8] we put forward in this section a simple theoretical approach that is able to describe,

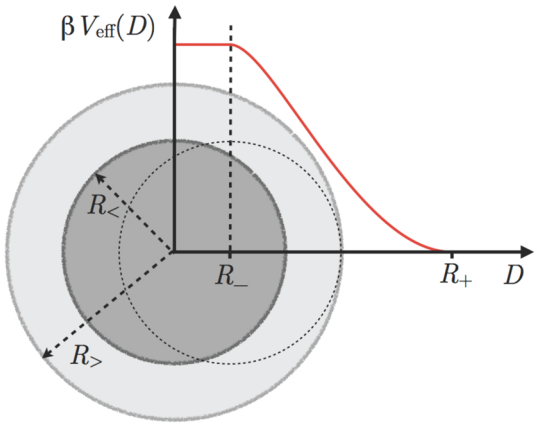

Figure 5. Scheme of the proposed model for the effective interaction between ring polymers. These are represented as two fully penetrable spheres of different radii, $R_>$ (light gray) and $R_<$ (dark gray). The accompanying plot shows the dependence of their overlap volume, assumed to be proportional to their effective interaction $\beta V_{\text{eff}}(D)$, on the separation D between their centers-of-mass. The effective potential is given by eq 19. For distances D smaller than R_-, there is full overlap between both spheres (see dotted circle representing the small ring at $D = R_-$). For distances larger than $D = R_+$, the overlap volume vanishes.

even semiquantitatively, the simulation results for the effective interaction $V_{\text{eff}}(R)$ between ring polymers. Consider two identical polymers, each with monomer density profiles $\rho(r)$ around their respective centers-of-mass. The case of dissimilar polymers can be treated in a similar fashion (see below). We introduce a corresponding dimensionless shape function $f(x)$, where x is the distance from the polymer center-of-mass scaled by its unperturbed radius of gyration, R_g^0. For simplicity we adopt the notation $R_g^0 = R_g$ in the following, and thus $x = r/R_g$. The density profile $\rho(r)$ and the shape function $f(x)$ are related as

$$\rho(r) \equiv \frac{N}{R_g^3} f(x) \tag{8}$$

Evidently, $4\pi \int_0^\infty x^2 f(x)\, dx = 1$. We assume an interaction between any two given monomers, at positions $\mathbf{r}_1$ and $\mathbf{r}_2$, of the excluded volume, contact type: $v_{\text{mm}}(\mathbf{r}_1 - \mathbf{r}_2) = v_0 k_B T \delta(\mathbf{r}_1 - \mathbf{r}_2)$. The excluded-volume parameter is $v_0 \propto \sigma^3$, where σ is the monomer size. Thus, this interaction corresponds to the case of polymers in athermal solvents, as those investigated here. The simplest approach to the calculation of the effective interaction between the two polymers, with their centers-of-mass held at separation $\mathbf{R}$, is a mean-field approximation (MFA). This expresses the effective potential as an overlap integral of the two density profiles, weighted by the excluded-volume interaction:

$$V_{\text{eff}}^{\text{MFA}}(R) \propto k_B T v_0 \int\int d^3\mathbf{r}_1 d^3\mathbf{r}_2 \delta(\mathbf{r}_1 - \mathbf{r}_2)\rho(|\mathbf{r}_1|)\rho(|\mathbf{r}_2 - \mathbf{R}|) \tag{9}$$

with some adimensional prefactor of order unity. Using eq 8, we readily obtain

$$V_{\text{eff}}^{\text{MFA}}(D) \propto k_B T \left(\frac{v_0}{\sigma^3}\right) N n \sigma^3 (f * f)(D) \tag{10}$$

where $D \equiv R/R_g$ is the normalized distance between the centers-of-mass of the two polymers. The quantity $n = N/R_g^3$ is the average monomer density within a polymer of volume $V_p \propto R_g^3$, and $f*f$ denotes the convolution of the two shape functions. Because of the assumed scaling behavior of f (see eq 8), this convolution is independent of the polymer size and also of order unity at full interpenetration ($D = 0$).

Equations 9 and 10 were first put forward by Flory and Krigbaum[19] for the derivation of the effective interaction between linear chains. By assuming a Gaussian distribution of the monomers around the centers-of-mass of two identical linear chains, the former scheme gave rise to a Gaussian effective interaction—the celebrated Flory–Krigbaum potential. However, the obtained prefactor of the potential was erroneous: as it is clear from eq 10 in association with the relation $n = N/R_g^{-3} \propto N^{1-3\nu}$ and the well-known scaling $R_g \propto N^\nu$ for self-avoiding chains (with $\nu \cong 3/5$ the Flory exponent), the so-obtained amplitude of the potential, $V_{\text{eff}}(D = 0)$, scales as $\sim N^{2-3\nu} \cong N^{1/5}$. If this result were correct, two linear chains would become more impenetrable by increasing their degree of

Table 1. Ring Topologies and Lengths Considered in the Simulations and the Theory of the Effective Interaction; Sizes of the Rings at Full Overlap ($D = 0$), As Obtained from the Simulations; Parameters of the Theoretical Model for the Effective Interaction, Obtained by Fitting the Simulation Results of $V_{\text{eff}}(D)$ to eq 19

polymer topologies and lengths		polymer sizes (simulation)		model parameters (theory)		
τ_A/τ_B	$N_A = N_B = N$	$R_>$	$R_<$	$R_>$	$R_<$	U_0
$0_1/0_1$	100	1.22	1.02	1.419	1.000	1.434
$0_1/3_1$	100	1.38	0.90	1.363	0.871	2.101
$0_1/3_1$	80	1.39	0.89	1.339	0.833	2.804
$0_1/3_1$	20	1.46	0.85	1.373	0.905	3.216

dx.doi.org/10.1021/ma4016483 | Macromolecules 2013, 46, 9437–9445

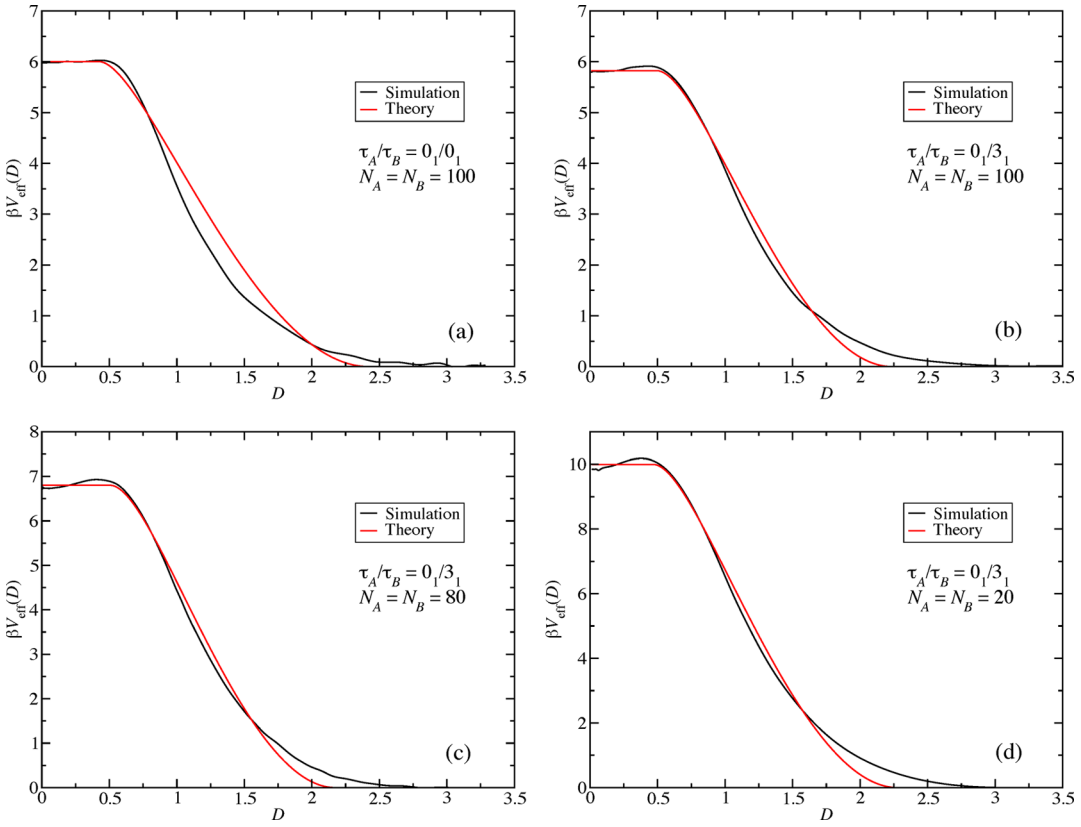

Figure 6. Effective potentials between ring polymers for various topologies and lengths (see legends). Black lines: simulation results. Red lines: theoretical descriptions by fitting to eq 19. The obtained fit parameters can be read off from the last three columns of Table 1.

polymerization (becoming fully impenetrable for $N \to \infty$). However, a series of theoretical and simulation studies have demonstrated that although the shape of the effective potential does fulfill the predicted Gaussian function, its amplitude is *independent* of N for sufficiently long chains ($N > N_L^*$).[5−16] Rather than a $\sim N^{1/5}$ dependence of the potential amplitude, it is found that $V_{eff}(D{=}0) \cong 2k_BT$.

The reasons lying behind the $V_{eff}(D{=}0) \sim N^{1/5}$ erroneous prediction were clarified by Grosberg et al.[8] In eq 10, the mean-field approximation assigns a probability p_c^{MFA} to each of the N monomers of a given polymer to have contacts with the monomers of the other, this probability being proportional to the packing fraction of the second one, Thereafter, a free energy cost proportional to k_BT times the number of contacts, $N(n\sigma^3)$, arises. The convolution $(f*f)(D)$ simply corrects for the overlap volume. This approach is, however, flawed in one very important way: in reality, monomer connectivity effects *reduce* the contact probability to[8]

$$p_c \propto (n\sigma^3)^{1/(3\nu-1)} \ll n\sigma^3 \tag{11}$$

and thus the correct expression for the effective potential reads

$$V_{eff}(D) \propto k_BT\left(\frac{v_0}{\sigma^3}\right)N(n\sigma^3)^{1/(3\nu-1)}(f*f)(D) \tag{12}$$

Since $n \propto N^{1-3\nu}$ (see above), and for large N the scaling function $f(x)$ only depends on the polymer architecture, it follows from eq 12 that in that limit $V_{eff}(D)$ scales as $\sim N^0$; i.e., it becomes independent of N. In particular, for linear chains $f(x)$ is a Gaussian function, and from eq 12 the well-known Gaussian interaction potential between self-avoiding chains comes out, with an amplitude $V_{eff}(D{=}0)$ of order k_BT. It is worth mentioning, however, that eq 10 has been shown to be quantitatively accurate for the case of interacting dendrimers.[33,34] In such systems the dense, regularly branched architecture of the molecules serves to restore the validity of the expression $p_c^{MFA} \propto n\sigma^3$. Thus, the effective potential between the centers-of-mass of dendrimers *does* depend on N, becoming steeper as the generation number grows.

In the following, we make use of eq 12 to obtain effective interactions for ring polymers, with the appropriate modifications of the shape functions $f(x)$ to take into account the effect of the polymer architecture on its size and shape. Before introducing the details of the model, we anticipate that eq 12 itself can rationalize the difference between the amplitudes $V_{eff}(D{=}0)$ of the effective potential for linear chains ($\cong 2k_BT$) and for unknotted rings ($\cong 6k_BT$). Thus, by using the relationship

$$R_g(\tau, N) = \lambda_\tau \sigma N^\nu \tag{13}$$

with some topology-dependent coefficient λ_τ, in conjunction with eq 12 and $n = NR_g^{-3}$, we find

$$\beta V_{eff}(D = 0) \propto \lambda_\tau^{-3/(3\nu-1)} \int d^3x f^2(x) \tag{14}$$

We assume that the major difference in the amplitude of the effective potential for different polymer architectures arises from the factor $\lambda_\tau^{-3/(3\nu-1)}$ and not from the convolution of the different shape functions at full interpenetration. With this approximation, the ratio Δ between the amplitudes of the effective potentials at $D = 0$ of the 0_1 rings and linear chains is given by

dx.doi.org/10.1021/ma4016483 | Macromolecules 2013, 46, 9437−9445

$$\Delta = \left(\frac{\lambda_L}{\lambda_{0_1}}\right)^{3/(3\nu-1)} \tag{15}$$

For the tethered model at hand, extensive simulations (results not shown) yield the values $\lambda_L = 0.533$ and $\lambda_{0_1} = 0.406$. By inserting these in eq 15 together with the precise value $\nu = 0.588$ for self-avoiding chains, we find $\Delta = 2.9$. This is indeed very close to the simulation result ($\Delta \approx 3$).

Consider now the application of eq 12 for the case of two different rings of sizes R_1 and $R_2 < R_1$. As discussed in section 3, this difference in size can arise in two different ways: first, if the two polymers have different architectures and/or degrees of polymerization (one is on average smaller than the other even at infinite separation), and second, if the two polymers are identical in N and τ, but one swells to facilitate penetration by the other. In either case, we denote $D \equiv R/R_g^0$ and define $R_> \equiv R_1/R_g^0$ and $R_< \equiv R_2/R_g^0$. It is also useful to define the sum and the difference between the sizes as $R_\pm \equiv R_> \pm R_<$ as well as the corresponding shape functions $f_>(x)$ and $f_<(x)$ of the large and small polymers, respectively. Although the sizes $R_>$ and $R_<$ do depend on the separation D, this dependence is weak for strong overlaps ($D \ll 1$). To simplify things, we thus keep them fixed for all distances at the values they have at $D = 0$ and generalize eq 12 to

$$V_{eff}(D) \propto k_B T (f_> * f_<)(D) \tag{16}$$

where we have now omitted the term $(v_0/\sigma^3)N(n\sigma^3)^{1/(3\nu-1)}$, which scales as N^0 (see above) and thus provides simply a constant factor of order unity.

The next approximation is inspired by the results of Figure 4b. There, it can be seen that for ring polymers the monomer distribution $\rho(r)$ strongly deviates from the Gaussian shape observed for linear chains (Figure 4a). Instead, by increasing r from zero it shows a roughly flat, or even increasing profile, until a pronounced decay is found for longer distances. Thus, we make a rather crude approximation for the shape functions of the rings, by modeling them as step functions:

$$f_\gamma(x) = \frac{3}{4\pi}\Theta\left(1 - \frac{x}{R_\gamma}\right) \tag{17}$$

where again $x \equiv r/R_g^0$, γ stands for > or < (large and small ring, respectively), and $\Theta(z)$ is the Heaviside step function. The shape functions defined in eq 17 fulfill the normalization condition

$$\int d^3x f_\gamma(x) = {R_\gamma}^3 \tag{18}$$

According to the definition of $R_{>,<}$ (see above), the right-hand side of eq 18 is identical to unity only if the two rings have equal sizes that do not change with separation. Obviously this is not the case, as has been shown in Figure 3. From eqs 16 and 17 we obtain the effective interaction as the overlap volume of spheres of unequal size, i.e.

$$\beta V_{eff}(D) = U_0 \begin{cases} \frac{4\pi}{3}{R_<}^3 & \text{if } 0 \le D < R_- \\ \frac{\pi}{12D}(D^2 + 2R_+D - 3{R_-}^2)(R_+ - D)^2 & \text{if } R_- \le D < R_+ \\ 0 & \text{if } R_+ \le D \end{cases} \tag{19}$$

where U_0 is a constant of order unity and the values of the parameters R_- and R_+ are determined as it will be specified below. The scheme of Figure 5 illustrates the relation between the shape of the effective interaction and the degree of overlap of the two spheres. As the separation D diminishes below R_+, the overlap increases. Full overlap is obtained at $D = R_-$, and this overlap remains invariant for all separations $D < R_-$, leading to a constant value of $V_{eff}(D)$ in that range. We can thus rationalize the plateau region observed in the effective potential as a direct consequence of the disparity in the sizes of the two rings at strong interpenetration. Even if the two rings have the same architecture and the same N, they adopt the (exchanging) roles of a large and a small one when their centers of mass are sufficiently close. The polymer architecture forces one of the two rings to strongly swell, accommodating the other. The flatness of $V_{eff}(D)$ at small D is then a direct consequence of this property, and it is absent for linear chains, which swell together at strong center-of-mass overlaps. Indeed, the latter feature a Gaussian effective potential, with a negative curvature at $D = 0$.

Now we test the analytical expression of eq 19 by comparing with the simulation results for the effective potentials of rings. The equation contains three free parameters: $R_<$, $R_>$, and U_0. However, there are strong constrains for their possible values. First, $R_>$ and $R_<$ should be consistent with the normalized radii of gyration of the large and small rings at full overlap ($D = 0$), which are independently obtained from the simulations. Second, in a scaling theory any missing coefficients (the constant U_0 in our case) should be numbers of order unity. Thus, we have fitted the simulation results for $V_{eff}(D)$ to eq 19, employing the Levenberg–Marquardt algorithm,[35] and constraining $R_<$ and $R_>$ to lie within small domains around the simulation values for the normalized radii of gyration. The obtained fit parameters are shown at the last three columns of Table 1, whereas the simulation values of the sizes are shown at the third and fourth columns.

The theoretical results for the effective interaction between rings are shown in Figure 6, where they are also compared with the simulation results. Semiquantitative agreement is found in all cases, and this is better for the case of mixed topologies ($\tau_A = 0_1, \tau_B = 3_1$) than for identical unknotted rings ($\tau_A = \tau_B = 0_1$). The main feature of the effective interaction between $0_1/0_1$ and $0_1/3_1$ ring polymer pairs, i.e., the plateau region for $0 \le D \lesssim 0.5$, is nicely reproduced. For the case of mixed topologies a very good description is also achieved up to separations $D \lesssim 1.7$. Moreover, the obtained values for the fit parameters $R_<$ and $R_>$ are in very good agreement with the normalized radii directly provided by the simulations (see Table 1), especially for the $0_1/3_1$ combinations. Consistently, the prefactor U_0 in eq 19 is of order unity in all cases. The main quantitative differences between the theoretical and simulation results of V_{eff} are observed at distance $D \gtrsim 1.7$. The model overestimates the late decay of the actual potential, which exhibits a longer tail. This discrepancy is a consequence of the oversimplification of the theoretical density profile, which has been modeled by a penetrable sphere with a sharp boundary, i.e., the step function in eq 17. Of course, the description of the actual effective potentials—e.g., accounting also for the local minimum at $D = 0$—might be improved by relaxing some of the rough approximations introduced in our model. More than to provide an accurate description, the purpose of our simple approach is to provide a direct connection between the particular shape of the effective potential and the architecture of ring polymers—

dx.doi.org/10.1021/ma4016483 | Macromolecules 2013, 46, 9437–9445

which force the large ring to swell in order to accommodate the small one at full interpenetration.

5. CONCLUSIONS

We have pointed out the differences in the effective potential between linear chains and ring polymers and investigated their microscopic origin. Swelling behavior is found for one or both polymers at strong interpenetration, i.e., at small separation between their centers-of-mass. However, the combination of polymer architecture and topological constraints have a very different effect on the swelling of linear and ring polymers. Two interpenetrating linear chains have the same average size, whereas in the case of ring polymers a depletion effect of the monomers of one ring from its own center of mass is found. One of the rings adopts an open conformation, leaving free space for accommodating the other one, which also swells with respect to its undistorted conformation but much less than the former. Thus, at full interpenetration the average sizes of the two rings are different, even if both rings have the same topology and degree of polymerization. We have modeled this depletion of monomers from the centers-of-mass of the rings by treating both rings as overlapping spheres of different size and considering connectivity and self-avoidance effects for the probability of monomer contacts. This simple approach provides a semiquantitative description of the effective potential for ring polymers and rationalizes the qualitative differences between the latter and the Gaussian potential for linear chains. Future work should focus on the possibilities to extend these considerations to knotted rings of complicated knotedness and to (semiflexible) rings carrying intramolecular stiffness.

AUTHOR INFORMATION

Corresponding Author

*E-mail: arturo.narros@univie.ac.at (A.N.).

Notes

The authors declare no competing financial interest.

ACKNOWLEDGMENTS

We acknowledge helpful discussions with Ronald Blaak. This work has been supported by the European Community's Seventh Framework Programme (FP7/2007-2013) under the IEF-RINGEFF, Grant Agreement 236664, and by the Austrian Science Fund (FWF), Grant 23400-N16.

REFERENCES

(1) Jang, S. S.; Çağin, T.; Goddard, W. A., III *J. Chem. Phys.* **2003**, *119*, 1843.
(2) Narros, A.; Moreno, A. J.; Likos, C. N. *Macromolecules* **2013**, *46*, 3654.
(3) Kapnistos, M.; Lang, M.; Vlassopoulos, D.; Pyckhout-Hintzen, W.; Richter, D.; Cho, D.; Chang, T.; Rubinstein, M. *Nat. Mater.* **2008**, *7*, 997.
(4) Bohn, M.; Heermann, D. W. *J. Chem. Phys.* **2010**, *132*, 044904.
(5) Narros, A.; Moreno, A. J.; Likos, C. N. *Soft Matter* **2010**, *6*, 2435−2441.
(6) Olaj, O. F.; Pelinka, K. H. *Makromol. Chem.* **1976**, *177*, 3413.
(7) Olaj, O. F.; Lantschbauer, W.; Pelinka, K. H. *Macromolecules* **1980**, *13*, 299.
(8) Grosberg, A. Y.; Khalatur, P. G.; Khokhlov, A. R. *Makromol. Chem., Rapid Commun.* **1982**, *3*, 709.
(9) Krüger, B.; Schäfer, L.; Baumgärtner, A. *J. Phys. (Paris)* **1989**, *50*, 3191.
(10) Louis, A. A.; Bolhuis, P. G.; Hansen, J. P.; Meijer, E. J. *Phys. Rev. Lett.* **2000**, *85*, 2522.
(11) Bolhuis, P. G.; Louis, A. A.; Hansen, J. P.; Meijer, E. J. *J. Chem. Phys.* **2001**, *114*, 4296.
(12) Bolhuis, P. G.; Louis, A. A. *Macromolecules* **2002**, *35*, 1860.
(13) Jusufi, A.; Dzubiella, J.; Likos, C. N.; von Ferber, C.; Löwen, H. *J. Phys.: Condens. Matter* **2001**, *13*, 6177.
(14) Louis, A. A.; Bolhuis, P. G.; Finken, R.; Krakoviack, V.; Meijer, E. J.; Hansen, J. P. *Physica A* **2002**, *306*, 251.
(15) Bolhuis, P. G.; Louis, A. A.; Hansen, J. P. *Phys. Rev. Lett.* **2002**, *89*, 128302.
(16) Krakoviack, V.; Hansen, J.-P.; Louis, A. A. *Phys. Rev. E* **2003**, *67*, 041801.
(17) Likos, C. N. *Phys. Rep.* **2001**, *348*, 267−439.
(18) Likos, C. N. *Soft Matter* **2005**, *2*, 478−498.
(19) Flory, P. J.; Krigbaum, W. R. *J. Chem. Phys.* **1950**, *18*, 1086.
(20) Bernabei, M.; Bacova, P.; Moreno, A. J.; Narros, A.; Likos, C. N. *Soft Matter* **2013**, *9*, 1287.
(21) Likos, C. N.; Lang, A.; Watzlawek, M.; Löwen, H. *Phys. Rev. E* **2001**, *63*, 031206.
(22) Likos, C. N.; Mladek, B. M.; Gottwald, D.; Kahl, G. *J. Chem. Phys.* **2007**, *126*, 224502.
(23) Lang, M.; Fischer, J.; Sommer, J.-U. *Macromolecules* **2012**, *45*, 7642.
(24) Reigh, S. Y.; Yoon, D. Y. *ACS Macro Lett.* **2013**, *2*, 296.
(25) Frank-Kamenetskii, M. D.; Lukashin, A. V.; Vologodskii, A. V. *Nature* **1975**, *258*, 398−402.
(26) Tanaka, F. *Prog. Theor. Phys.* **1982**, *68*, 148−163.
(27) Iwata, K.; Kimura, T. *J. Chem. Phys.* **1981**, *74*, 2039−2048.
(28) Hirayama, N.; Tsurusaki, K.; Deguchi, T. *J. Phys. A: Math. Theor.* **2009**, *42*, 105001.
(29) Marenduzzo, D.; Orlandini, E. *JSTAT: Theory Exp.* **2009**, L09002.
(30) Schäfer, L.; Krüger, B. *J. Phys. (Paris)* **1988**, *49*, 749.
(31) Marcone, B.; Orlandini, E.; Stella, A. L.; Zonta, F. *Phys. Rev. E* **2007**, *75*, 041105.
(32) Capone, B.; Coluzza, I.; Lo Verso, F.; Likos, C. N.; Blaak, R. *Phys. Rev. Lett.* **2012**, *109*, 238301.
(33) Likos, C. N.; Rosenfeldt, S.; Dingenouts, N.; Ballauff, M.; Werner, N.; Vögtle, F. *J. Chem. Phys.* **2002**, *117*, 1869.
(34) Götze, I. O.; Harreis, H. M.; Likos, C. N. *J. Chem. Phys.* **2004**, *120*, 7761.
(35) Press, W. H.; Teukolsky, S. A.; Vetterling, W. T.; Flannery, B. P. *Numerical Recipes*; Cambridge University Press: New York, 1992.